Experimental Measurements of a Liquid Droplet Impinging on a Corrugated Cardboard Surface

Xiangyang Zhou
FM Global, 1151 Boston-Providence Turnpike, Norwood, MA, USA
xiangyang.zhou@fmglobal.com

Abstract

In order to provide data suitable to validate a water-based fire protection model, measurements were conducted to study the impingement process of a liquid droplet upon a corrugated cardboard surface. The amount of mass converted to secondary droplets due to splashing was measured by a weighing balance. The size, velocity and number density of the splashed droplets was measured by a laser-based Shadow-Imaging system. The impact surface was dry unheated cardboard of the kind that is widely used in corrugated boxes and shipping containers. Two liquids, with different surface tension, three droplet sizes, three impact angles and different impact velocities were investigated. Based on the measurements, a critical Weber number was introduced to determine the transition from deposition to splashing. The splashing fraction was expressed as a function of Weber number and impact angle. The distribution of cumulative volume fraction of splash droplets versus a normalized droplet size was correlated as a Rosin-Rammler function. The volume-median droplet diameter was expressed as a function of Weber number and impact angle. The maximum velocity magnitude of a splash droplet was correlated to its diameter and Weber number. These empirical correlations can be incorporated into a numerical model to simulate the splashing fraction, size and velocity distributions of the splashed droplet.

Introduction

The impingement of liquid droplets on a solid or liquid surface is important in many engineering applications. In a sprinkler-based fire protection system, part of the water droplets from a sprinkler spray can penetrate through the fire plume and impinge on the surface of the fuel such as a corrugated cardboard box. Droplet impingement can also occur during water transport through a rack storage arrangement. Regarding a single droplet impinging on a surface, three different outcomes of this impact are possible: (1) the droplet may deposit on the surface and form a water film, (2) for higher momentum impacts, the impinging droplet may splash, leading to a cloud of smaller secondary droplets around the point of impingement, and (3) for special surface conditions, such as on very hot surfaces, the droplet may be completely reflected. These outcomes can change the amount of water transported along the fuel surface. Since water cooling of a fuel surface is the dominant mechanism for sprinkler protection, the amount of water droplets deposited on the fuel surface is of considerable importance.

Droplet-surface interaction is a complex process. The possible outcomes of deposition, splashing or rebound are controlled by a number of parameters, including: liquid droplet properties (i.e., density, surface tension, and viscosity), droplet size, droplet impact velocity and contact angle, and fuel surface characteristics such as roughness, softness, wettability, temperature, and whether the surface is dry or wet. The complicated physics associated with all the interactions is not yet well understood despite numerous experimental and theoretical studies that have been performed in the past [1-12]. A major challenge to the understanding of this droplet-surface interaction is its inter-disciplinary, non-linear and stochastic nature.

The characteristics of an impacted surface are important and affect the outcome of a liquid droplet impinging on a surface. The collision dynamics of the impact droplet on different surfaces can be vastly distinct. Literature review shows that there are many previous studies of liquid droplets impinging on different solid surfaces [1-6], or on liquid layers of different depths [7-12]. Although numerous studies have been performed, no measurements are reported on spray droplets impinging on a corrugated cardboard box, typically used for storing commodities in racks. FM Global is developing a new computational code, FireFOAM, to model water-based fire protection [13]. A film-transport model has been developed for this code to simulate water transport on a solid fuel surface where impingement, splashing, and film separation processes are all considered. However, the film transport model still requires experimental guidance and certain empirical inputs such as splashing mass fraction.

The goal of the present investigation is to provide experimental data in a form suitable to validate and improve the film transport model on corrugated cardboard surfaces used in FireFOAM. For this purpose the size and velocity distributions of the secondary droplets and the splashing mass fraction were measured in a range of parameters relevant to sprinkler protection. The droplet size, impact velocity, impact angle, and liquid surface tension were varied. A laser-based Shadow-Imaging system was employed, in addition to other measuring and visualization techniques. Due to limited space, this paper only presents measurements on a dry unheated cardboard surface. Empirical correlations

were developed to describe the splashing mass fraction as well as the size and velocity distributions of the splashed droplets.

Experimental Setup

The liquid droplets were generated using a syringe pump that was controlled to dispense the liquid at a steady rate of 100 mL/hour. The droplet was formed at the tip of the needle and detached under its own weight. The droplet size was changed by using different needles. The height of the needle above the surface was adjusted to change the droplet impingement velocity. To evaluate the effect of the liquid surface tension on the impingement, two liquids with different surface tensions were used. One is deionized (DI) water that has a surface tension of 0.0728 N/m at 20°C. The second is a blend of Ethanol (11.1% in mass fraction) and DI water. The surface tension of the blend is 0.047 N/m at 20°C [14], which is 35.4% smaller than that of DI water. The density of the blend is 0.974 g/cm^3, as calculated from the mass composition. It is 2.3% lower than that of DI water (0.998 g/cm^3) at 20°C. The kinematic viscosity of the blend was estimated to be 1.047×10^{-6} m^2/s using the Refutas equation [15]. This value is 4.3% higher than that of DI water (1.004×10^{-6} m^2/s) at 20°C.

Figure 1 shows a solid surface sample that was cut from a triple-wall corrugated cardboard. Cardboard is a paper-based material consisting of fluted corrugated sheets, intermediate plies and flat linerboards. It is widely used in the manufacture of corrugated boxes and shipping containers. The roughness, softness and wettability of the cardboard surface are expected to be different from that of other materials such as metal, glass or ceramic, which have been studied extensively in literature. The water absorption propensity of four different corrugated cardboards was measured in reference [16]. In general, water absorption rate for a corrugated board increases linearly with water flux, and is slightly affected by the surface characteristics and morphology of the board.

A small cardboard sample, 35 mm in diameter and 14 mm in thickness, was used in this work for the splashing measurement. It was set up in the experiment so that a falling liquid droplet would impinge on the center of the cardboard sample. A new sample was used for each experiment. The sample size was selected to collect the deposited liquid. The impact angle was defined with respect to the normal direction of the surface. For example the impact angle of a falling droplet is zero on a horizontal surface. Because it is not easy to control the direction of a falling droplet, the impact angle was changed in this work by inclining the cardboard surface.

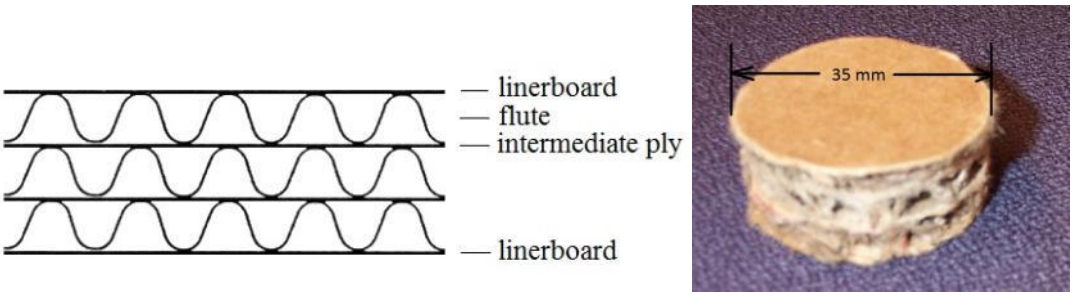

Figure 1 Illustration of a triple-wall corrugated cardboard and a sample for the current test.

The laser-based Shadow-Imaging system was used to measure droplet size and velocity. This system was previously used to measure sprinkler sprays [17]. It is based on the shadowgraph technique with high-resolution imaging and pulsed backlight illumination. The light source is a double-cavity-frequency Nd:YAG laser, which provides two light pulses of 532 nm wavelength, each with a pulse energy of about 120 mJ at 15 Hz double-pulse rate. The camera detection system consists of a 14-bit dual-frame CCD camera with a 2048×2048 pixel resolution, and a 12X zoom system that can achieve a field of view down to 400 μm. Using a short laser pulse (less than 16 ns) as illumination, the exposure time is so small that a moving droplet is "frozen" and the droplet size can be measured. A two-dimensional velocity is measured from the shift distance of droplets recorded in a pair of images with a known time interval. A double-pulse laser combined with a double-frame camera allows for the investigation of droplet size, velocity and size-velocity dependency.

After calibrating the detection system, the current camera's field of view was 31.6×31.6 mm. The minimum droplet size that could be detected was 80 μm. During the test, the digital camera focused on the impingement location and the impact droplet fell through the vertical focal plane. The statistical results were calculated from the attributes of all the detected droplets. One of the characteristic droplet diameters is the volume-median droplet diameter, d_{v50}, which denotes that 50% of the cumulated water volume is represented by droplets having a diameter smaller than d_{v50}.

For understanding the droplet impingement process, a high-speed digital camera at 1000 frames/s with an exposure time of 250 μs was also used. Each image has a pixel resolution of 1504×1128. The physical size of the camera field view was adjusted to be 64×48 mm. For a droplet impinging on a dry surface in a period of about 50 ms, this camera can visualize the entire impingement process, and be used to determine the boundary between droplet deposition and splashing.

A large single droplet relevant to sprinkler spray was selected for the current study. For DI water, two sizes of droplets were generated with diameters of 4.3±0.1 and 2.9±0.1 mm from different needles. For the blend liquid of Ethanol plus DI water, the generated droplet size was 4.2±0.1 mm. The impact droplet velocity was varied in a range from 1.5 to 3.7 m/s by adjusting the falling height from 0.11 to 0.76 m. The size and velocity of droplets generated from the needle were also measured by the Shadow-Imaging system.

The experimental setup illustrated in Figure 2 was designed to measure the splashing mass fraction. The cardboard sample was placed in the center of a pan and a cover plate. There is a gap of about 4 mm between the sample and the cover plate. The cover plate is 2 mm lower than the cardboard sample surface. When a falling droplet impinges on the cardboard surface, the splashed liquid is collected by the plate, and the deposited liquid is collected by the cardboard and the pan. The splashing mass fraction is calculated as:

$$Y_{splash} = \frac{m_{impinge} - m_{deposit}}{m_{impinge}}, \quad (1)$$

where $m_{impinge}$ is the mass of the impact droplet, and $m_{deposit}$ is the mass of liquid deposited on the cardboard sample. A precision weighing balance with a capacity of 210 g and a standard deviation of 0.1 mg was used to measure the mass difference.

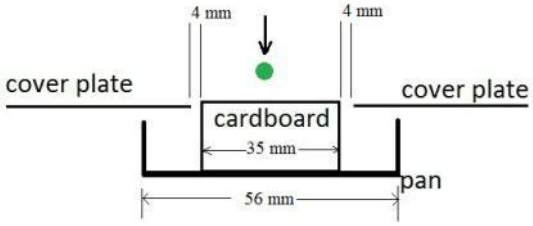

Figure 2 A sketch of an experimental setup to measure the splashing mass fraction.

The test matrix involved two liquids, three droplet sizes, three impact angles and various impact velocities. Each test case was repeated at least three times. The temperatures of water and the cardboard surface were not controlled and were approximated to be the room temperature of about 20 °C.

Results and Discussion

There are many parameters influencing the outcome of a droplet impact on a surface. The influential parameters are often combined to yield the dimensionless parameters essential to the description of the impingement process. The first important parameter for the current work is the droplet Weber number, representing the ratio of inertia to surface tension forces, given as

$$\mathrm{We} = \rho V_{I,n}^2 d_I / \sigma \quad (2)$$

where ρ is the liquid density, $V_{I,n}$ is the surface-normal incident velocity of the impinging droplet, d_I is the diameter of the impinging droplet, and σ is the liquid surface tension. Another dimensionless parameters is the droplet Laplace parameter

$$\mathrm{La} = \rho \sigma d_I / \mu^2 \quad (3)$$

where μ is the liquid viscosity. This parameter represents the ratio of surface tension forces to viscous forces in the droplet. Other parameters such as the Reynolds number ($\mathrm{Re} = \rho V_{I,n} d_I / \mu$) and the Ohnesorge number ($\mathrm{Oh} = \mu / \sqrt{\rho \sigma d_I}$) have also been often used in previous investigations.

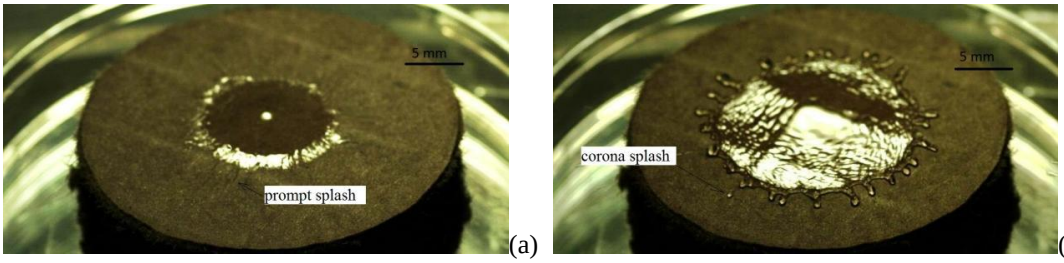

(a) (b)

Figure 3 Time-lapse images of a water droplet (d_I=4.3 mm, $V_{I,n}$=3.1 m/s) impingement upon a dry cardboard surface: (a) 1 ms and (b) 5 ms.

Using the high-speed camera, Figure 3 displays the time-lapse images of a water droplet impingement on a dry cardboard surface. At t=1 ms after the droplet touches the surface impact, Figure 3(a) shows that the droplet is deformed as a plain water film in a solar corona shape. The corona's diameter is about 11 mm. Prompt splashing is observed at this time with some small secondary droplets being created. Under the effect of the initial momentum, the water film spreads outwards and the corona size grows in time. At t=5 ms, as shown in Figure 3(b), the corona reaches its maximum size of about 18 mm. During this spreading process, the water film becomes thinner. Because of the shear stress of the rough cardboard surface, the spreading water film also becomes unstable. Figure 3(b) shows that the instability develops in the form of fingers when the corona grows. Some fingers detach from the surface and break up into a number of secondary droplets, denoted as a corona splash.

To determine the transition from deposition to splashing, an empirical criterion was developed using the critical Weber number [12] as:

$$\mathrm{We_c} = \Lambda \cdot \mathrm{La}^{-0.183}, \tag{4}$$

where Λ is an empirical factor that depends on surface roughness. This factor Λ typically ranges from 1300 to 5200, and decreases with increasing surface roughness [12]. For $We<We_c$, a droplet will deposit on the dry wall. For $We>We_c$, the droplet impingement will result in splashing. Another criterion is given in terms of the Re and Oh numbers [1] by the relation $\mathrm{K} = \mathrm{Re} \cdot \mathrm{Oh}^{1.25}$. A value of K exceeding 57.7 leads to splashing, whereas K less than 57.7 leads to complete deposition of the liquid droplet.

For the current cardboard surface in a limited range of test conditions, the deposition-splashing transition was observed by the high-speed camera and also the Shadow-Imaging system. Several tests were conducted by changing the impact velocity while keeping other parameters constant. Table 1 presents the observed splashing results, in which the splashing occurred when one or more secondary droplets were observed.

To fit the correlation expressed by the critical Weber number, the surface roughness factor is assumed to be Λ=1770. Under this assumption, Table 1 shows that no-splashing occurred at $We<We_c$, and splashing occurred at $We>We_c$. The second criterion given by the relation K=57.7 failed for three of the test conditions, where no-splashing was observed in spite of the fact that K was equal to or greater than 107. It is postulated that this criterion failed, for the current cardboard surface, because surface characteristics such as roughness were not included.

Table 1. The deposition-splashing transition observed for different droplets and velocities.

Liquid	d_l *(mm)*	$V_{l,n}$ *(m/s)*	*We*	*Re*	*Oh*	*La*	*K*	We_c	Splashing
Water	4.368	1.53	141	6670	0.0018	3.2×10^5	107	174	No
Water	4.368	1.72	176	7463	0.0018	3.2×10^5	123	174	Yes
Water	2.916	1.97	156	5741	0.0022	2.1×10^5	109	187	No
Water	2.916	2.17	188	6302	0.0022	2.1×10^5	122	187	Yes
Ethanol+ Water	4.240	1.46	188	5942	0.0023	1.9×10^5	120	192	No
Ethanol+ Water	4.240	1.53	205	6208	0.0023	1.9×10^5	127	192	Yes

The transition results observed so far are restricted to a limited range of conditions. Before more theoretical and experimental investigations are conducted, the criterion given by the critical Weber number, with a roughness factor of Λ=1770, can be used to describe the transition from deposition to splashing on a dry cardboard surface.

Although the transition from deposition to splashing was examined in these tests, the amount of mass converted to secondary droplets due to splashing was not measured. Since this quantity is very important for the purpose of tracking water transport on fuel surfaces, the splashing fractions were measured using the setup shown in Figure 2. Each test was designed to impinge one droplet on a dry cardboard surface and then to measure the mass difference. Figure 4 presents the average values of the splashing fraction measured at different impact velocities for two liquids, three droplet sizes, and three impact angles. The standard deviations are illustrated as error bars. The average values and the standard deviations were calculated from three repeated test results. All the data were plotted versus the Weber number. For an inclined surface with an angle of θ, the Weber number was calculated using the normal velocity component. To correlate the test data with different impact angles, the Weber number was multiplied by a fitting factor of $1 + 2\sin(\theta)$.

Based on the measurements, a fitting function was developed as:

$$\mathrm{Y_{splash}} = 7.9\ln[\mathrm{We}(1 + 2\sin\theta)] - 43.2, \tag{5}$$

which correlates the splashing fraction with the Weber number and the impact angle in the current test range of $300<We<1200$ and $0°\leq\theta\leq30°$. Figure 4 also shows that the measured splashing fractions are scattered and not well repeated for some test cases. This is because the impingement is a stochastic process and the surface properties of each cardboard sample may not be uniform. Generally, the splashing fraction on a dry cardboard surface is small (<14%).

For the same droplet impinging on an inclined surface, the splashing fraction is generally larger than that on a flat surface. The effect of impact angle may come from the asymmetry of a spreading liquid sheet resulting from the oblique angle of impact. When a droplet does not impact normal to a surface, its increased tangential momentum may increase the instability of the spreading film, and hence enhance fragmentation of the droplet.

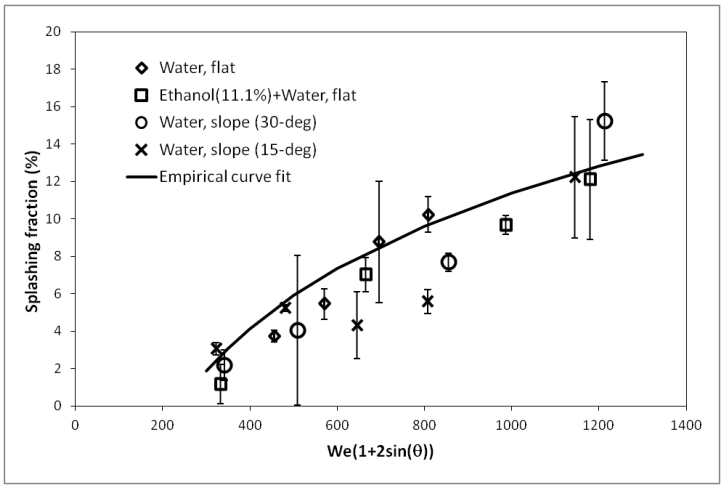

Figure 4 Splashing fraction and empirical curve fit measured for different test conditions.

The size and velocity of splashed droplets were measured using the Shadow-Imaging system. Figure 5 shows two images of splashed droplets captured at two times after a water droplet impinged on a dry cardboard surface. The impact droplet had a diameter of 4.3 mm and a velocity of 3.7 m/s. The arrow vector in the figure represents the falling trajectory of the impact droplet. Because the field of view of the camera is small, only half of the impingement is recorded in the image. Figure 5 shows that many secondary droplets are splashing from the center at a small angle relative to the horizontal surface. The size and velocity of these splashed droplets were detected and calculated using post-processing software. At t=4 ms, there are 26 droplets being detected in the image. The size range is 0.09–0.33 mm and the speed range is 2.1–6.8 m/s. Most of secondary droplets have a speed higher than that of the primary droplet. At a later time of t=10 ms, there are 16 droplets being detected. The size range is 0.11–0.64 mm and the speed range is 0.5–2.3 m/s. At these two stages, the size and velocity of secondary droplets are different, with the droplets at later times fewer in number but larger and slower. This result was also observed for other impact conditions. The possible reason is that secondary droplets at different stages are created by different mechanisms. These splashed droplets will be entrained by the air flow or end up on a large cardboard surface.

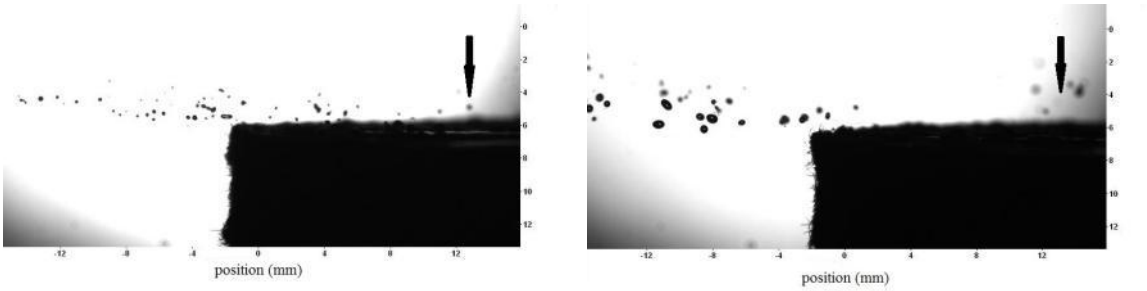

Figure 5 Shadow images of splashed droplets captured at t=4 ms (left) and t=10 ms (right) after water droplet (d_I=4.3 mm and $V_{I,n}$=3.7 m/s) impingement on the cardboard surface.

Figure 6 shows a shadow-image of splashed droplets captured at t=4 ms for a water droplet impinging on a 30° inclined dry surface. The impact droplet has the same characteristics as those shown in Figure 5. At this early stage, Figure 6 shows that many small secondary droplets fly downward along the inclined surface and some big droplets are shedding from the spreading liquid film. It is also observed that the spreading liquid film on the inclined surface is not symmetrical. Most of the secondary droplets are seen to splash to the downside; therefore, the measuring location (or the focal plane) was selected at the downside of impingement for tests with an inclined surface.

Statistical results are calculated from a number of detected secondary droplets. Generally, all else being equal, a larger sample size leads to increased precision in estimates of various statistical properties. However, a larger sample size means more images are needed because the number of detected droplets in each image is about ten or less. For each dry sample, the current Shadow-Image system can capture only a pair of images at one time. Therefore, a tradeoff was made by capturing 30 pairs of images, in total, at two times for each impinging condition. However, statistic-

al properties were calculated only when the number of detected droplets exceeded 200. A statistical calculation of a normal distribution showed that the sampling error was 7% with a 95% confidence interval when the sampling size was n=200. In statistics, sampling error is the error caused by observing a sample instead of the whole population.

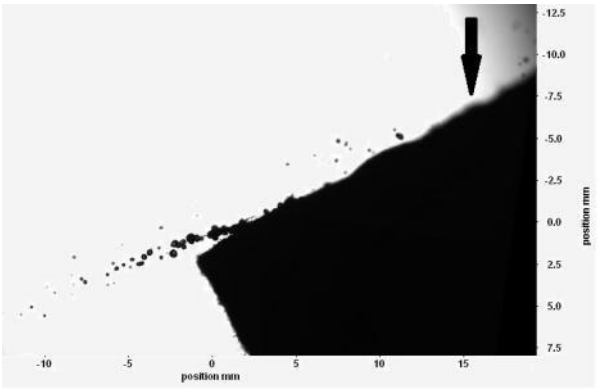

Figure 6 A shadow-image of splashed droplets captured at t=4 ms after water droplet impingement on a dry cardboard surface with an impact angle of 30°.

Figure 7 shows the distributions of cumulative volume fraction (CVF) of splashed droplets versus the normalized droplet size d/d_{v50}, where d_{v50} is the volume-median droplet diameter. For two liquids, three droplet sizes, three falling velocities and three impact angles, these data were measured for a single droplet impinging on a dry cardboard surface. A Rosin-Rammler fitting function was developed to correlate the droplet size distribution as:

$$F(d) = 1 - \exp\left[-0.693\left(\frac{d}{d_{v50}}\right)^{2.8}\right], \quad (6)$$

where F(d) is the CVF of splashed droplets with a diameter less than d. Under different impinging conditions, Figure 7 shows that the distribution of the splashed droplet sizes can be correlated by a Rosin-Rammler function.

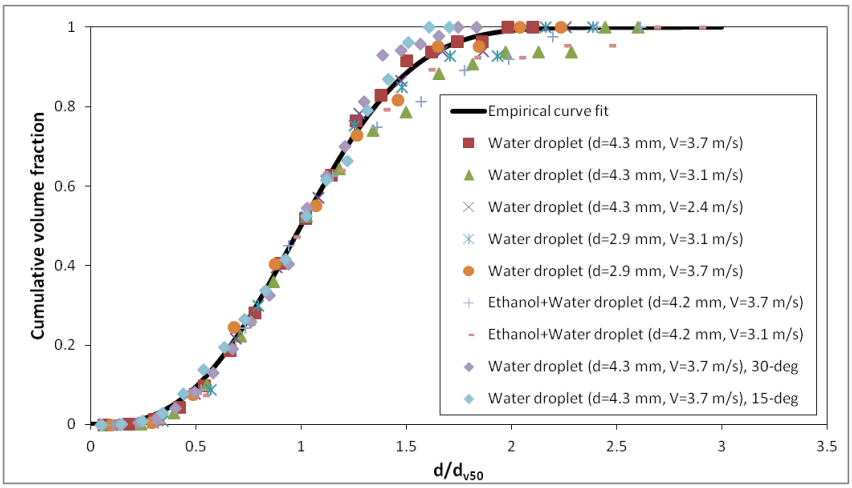

Figure 7 CVF distributions of splashed droplets fitted with a Rosin-Rammler function and measurements obtained from a droplet impinging on a dry cardboard surface for different liquids, sizes, velocities and impingement angles.

The volume-median droplet diameter d_{v50} varies for different impact conditions. Figure 8 presents the distribution of d_{v50} versus the Weber number, where d_{v50} is normalized by d_I (size of the impact droplet), and the Weber number is multiplied by a factor of $1 + 2\sin(\theta)$ for an impact angle of θ. The line plotted in the figure is a fit described by the following function:

$$\frac{d_{v50}}{d_I} = 0.0474 ln[We(1 + 2sin\theta)] - 0.2134 \quad , \quad (7)$$

which was developed to correlate the volume-median diameter of splashed droplets to Weber number and impact angle in the current test range of 300<We<900 and 0°≤θ≤30°. However, this function is only applicable for water droplets and not the blend liquid. Figure 8 shows that the values of d_{v50} of a blend liquid (Ethanol+Water) are lower than those of water droplets. The possible reason is that the surface tension of the blend liquid is 35.4% lower than that of water.

This parameter characterizes the forces that resist the formation of additional surface area. Thus a liquid film with small surface tension is easy to deform and breakup into small secondary droplets. More measurements are still needed to correlate d_{v50} for different liquids or water of varying surface tension.

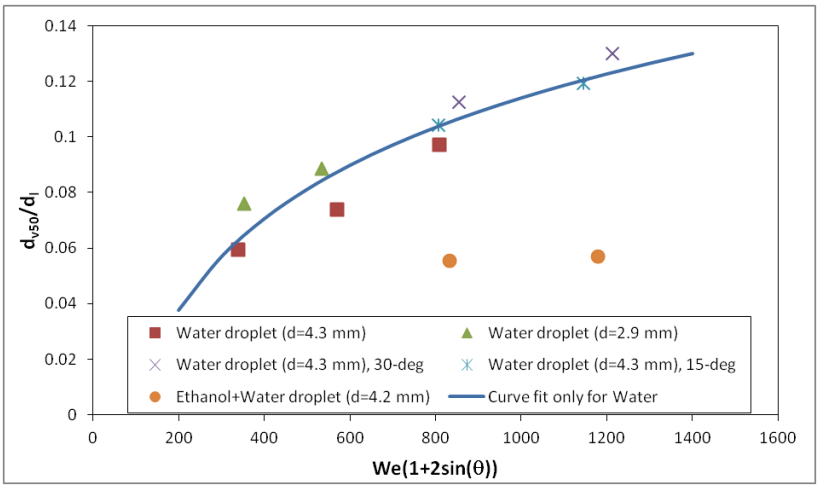

Figure 8 Normalized volume-median diameter of splashed droplets versus Weber number and impact angle measured for single droplet impingement on a dry cardboard surface.

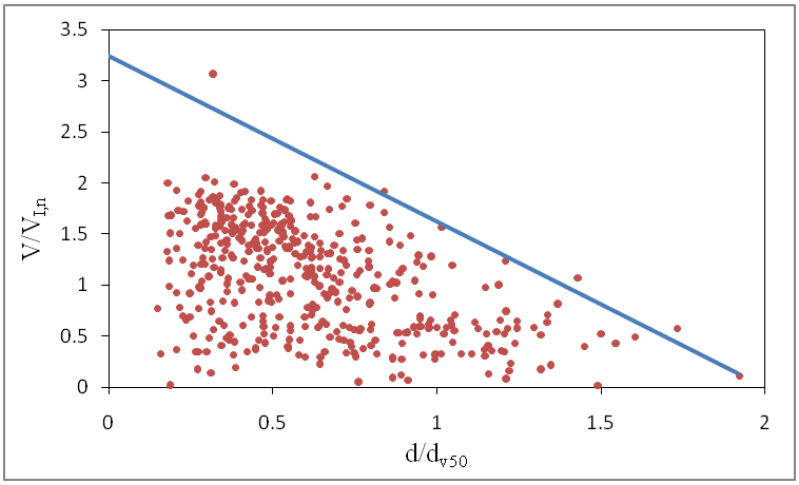

Figure 9 Scatter plot of normalized droplet velocity magnitude *versus* normalized droplet diameter for the impingement of a water droplet (d_I=4.3 mm, $V_{I,n}$=3.7 m/s).

The velocity distribution of a splashed droplet is complicated because both magnitude and direction should be determined. Figure 9 shows a scatter plot of splashed droplet velocity magnitude versus normalized droplet diameter for a water droplet (d_I=4.3 mm, $V_{I,n}$=3.7 m/s) impinging on a dry cardboard surface. A general trend is that small droplets tend to have higher velocity. If each secondary droplet is assumed to have the same kinetic energy after the impingement, it is reasonable that a small droplet would have a higher velocity. For other impact droplets at different conditions, it is observed that the velocity scatter plots are similar. Figure 9 also illustrates a straight line that represents a possible maximum velocity magnitude for a droplet size. This line is expressed as a function:

$$\frac{V_m}{V_{I,n}} = 0.5C_W\left(2 - \frac{d}{d_{v50}}\right) \text{ for } 0 < \frac{d}{d_{v50}} < 2, \quad (8)$$

which is used to correlate the maximum velocity magnitude (V_m) to a droplet size. Because smaller splashed droplets tend to lose momentum faster than the larger droplets, the straight line in Figure 9 attempts to correlate the velocities of the small droplets with d/d_{v50}<0.5. The coefficient C_W is correlated as a function of Weber number as:

$$C_W = -0.84\ln(We) + 8.8, \quad (9)$$

which is applicable for different droplets impinging on a dry cardboard surface in the current test range. For an inclined surface, the Weber number is calculated using the normal velocity component. When the impact condition is determined, the value of V_m can be calculated for a droplet size. Assuming a uniform distribution in probability density, the droplet's velocity magnitude can be selected randomly in the range from 0 to V_m.

The flight direction of splashed droplets is almost parallel to the surface level, as shown in Figures 5 and 6. There is a small elevation angle of about 7°. Therefore, the velocity vector direction can be approximated as a random elevation angle in the range from 0° to 7°. However, the azimuthal distribution of the velocity vector around the impact center is more complicated. If a droplet impinges normal to a horizontal surface, the azimuthal distribution can be assumed to be uniform. If an inclined surface is impacted, the velocity magnitude will be a function of the azimuthal angle. Generally the maximum velocity magnitude appears at the slope downside of the impact location and the minimum at the upside of the impact location. Further research is needed to quantify this azimuthal distribution.

Summary and Conclusions

Measurements were conducted to study the impingement process of a liquid droplet upon a dry unheated cardboard surface. Based on the measurements, empirical correlations were introduced to determine the transition from deposition to splashing, and to describe the splashing mass fraction as well as the size and velocity distributions of the splashed droplets. These correlations can be incorporated into the numerical model to simulate the dynamics of droplets splashing on a dry cardboard surface. The current measuring conditions are idealized for a single droplet and not a cloud of droplets, such as that generated by an automatic fire sprinkler. Furthermore, the investigated parameters were limited and some phenomena such as fluid flow, heat transfer and liquid evaporation relevant to droplet impingement were not included in the present work. This will be the subject of further investigations.

Acknowledgements

This study was funded by FM Global in its sprinkler technology research program. The author is grateful to Regis Bauwens, Stephen D'Aniello, Blair Swinnerton and Geary Yee for their assistance in the preparation of the measurement setup. The discussions with Yibing Xin, Hong-Zeng Yu, Karl Meredith, Christopher Wieczorek and Franco Tamanini are also appreciated.

References

[1] Mundo, C., Sommerfeld, M. and Tropea, C., Droplet-wall collisions: experimental studies of the deformation and breakup process. *Int. J. Multiphase Flow*, Vol. 21, 1995, pp. 151–173.

[2] Range, K. and Feuillebois, F., Influence of Surface Roughness on Liquid Drop Impact, *J. Colloid and Interface Science*, Vol. 203, 1998, pp. 16–30.

[3] Rioboo, R., Marengo, M. and Tropea, C., Time evolution of liquid drop impact onto solid, dry surfaces, *Experiments in Fluids*, Vol. 33, 2002, pp. 112–124.

[4] Roisman, I.V., Rioboo, R. and Tropea, C., Normal impact of a liquid drop on a dry surface: model for spreading and receding, *Proc. R. Soc. Lond.* A (2002) 458, 1411–1430.

[5] Josserand, C., Lemoyne, L., Troeger, R. and Zaleski, S., Droplet impact on a dry surface: triggering the splash with a small obstacle, *J. Fluid Mech*., Vol. 524, 2005, pp. 47–56.

[6] Gipperich, A., Lembach, A.N., Roisman, I.V. and Tropea, C., On the Splashing Threshold of a Single Droplet Impacting onto Rough and Porous Surfaces, *ILASS – Europe 2010, 23rd Annual Conference on Liquid Atomization and Spray Systems*, Brno, Czech Republic, September 2010

[7] Harlow, F.H. and Shannon, J.P. The Splash of a Liquid Drop, *Journal of Applied Physics*, Vol. 38, 1967, pp. 3855-39867.

[8] Macklin, W.C. and Metaxas, G.J., Splashing of drops on liquid layers. *J. Appl. Phys*., Vol. 47, 1976, pp. 3963–3970.

[9] Rein, M., Phenomena of liquid drop impact on solid and liquid surfaces. *Fluid Dynamics Research*, Vol. 12, 1993, pp. 61-93.

[10] Cossali, G.E., Coghe, A. and Marengo, M., The impact of a single drop on a wetted surface, *Experiments in Fluids*, Vol. 22, 1997, pp. 463–472.

[11] Manzello, S.L. and Yang, J.C., An experimental study of a water droplet impinging on a liquid surface, *Experiments in Fluids*, Vol. 32, 2002, pp. 580–589.

[12] Bai, C.X., Rusche, H. and Gosman, A.D., Modelling of gasoline spray impingement. *Atom. Sprays*, 12:1–27, 2002.

[13] Wang, Y., Chatterjee, P. and de Ris, J.L., Large eddy simulation of fire plumes, Proceedings of the Combustion Institute, Volume 33, Issue 2, 2011, pp 2473–2480.

[14] Dean, J. A. and Lange, N. A., *Lange's Handbook of Chemistry*, pp 1661–1665, ISBN 0070161909, New York: McGraw Hill Book Company (1967, 11th ed.).

[15] Maples, R. E., *Petroleum Refinery Process Economics* (2000, 2nd ed.). Pennwell Books. ISBN 0878147799.

[16] JAYAWEERA, T.M. and Yu, H-Z, Water Absorption in Horizontal Corrugated Boards Under Water Sprays, *Fire Safety Journal*, vol. 41, pp. 335-342, 2006.

[17] Zhou, X. and Yu, H. Z., Experimental Investigation of Spray Formation as Affected by Sprinkler Geometry, *Fire Safety Journal*, 46 (2011) 140–150.